MDPI

Article

Moisture buffering in surface materials due to simultaneous varying relative humidity and temperatures. Experimental validation of new analytical formulas

Valeria Cascione [1,†],Carl-Eric Hagentoft [2,‡], Daniel Maskell [3,†], Andy Shea [4,†*] and Pete Walker [5,†]

[1] v.cascione@bath.ac.uk
[2] carl-eric.hagentoft@chalmers.se
[3] d.maskell@bath.ac.uk
[4] a.shea@bath.ac.uk
[5] p.walker@bath.ac.uk
* Correspondence: a.shea@bath.ac.uk
† Department of Architecture and Civil Engineering, University of Bath, Bath, UK
‡ Building Technology, Department of Architecture and Civil Engineering, Chalmers University of Technology, Göteborg, Sweden

Version 28th October 2020 submitted to Appl. Sci.

Abstract: Buildings are subjected to the indoor environment, especially in non-controlled climates. Temperature and humidity variations might effect or even damage materials sensitive to moisture. For this reason, it is important to understand the response of hygroscopic materials to variable indoor environmental conditions. Existing methods looked into the dynamic sorption capacity of materials, by analysing the impact of only humidity fluctuations, with temperature usually considered non-influential or non variable. However, temperature fluctuations may impact the moisture capacity of the materials, as materials properties might substantially vary with temperature. Moreover, in existing protocols the humidity variations are considered varying under square wave fluctuations, which may not be applicable in environments, where the indoor is influenced by daily and seasonal climate variations, which presents more complex fluctuation. In this study a simulation method that can predict the impact of environmental condition on materials under simultaneous temperature and humidity fluctuations was developed. Clay and gypsum plaster were analysed in the numerical model and results were then validated with experimental data. Materials were subjected to either sinusoidal and triangular temperature and RH variations and different cycle time intervals. The investigation of sinusoidal and triangular environmental variations pushed to a better understanding of materials response to different environments and to the improvement of the simplified model. The development of a simplified model can realistically predict the potential future impact of climate changes on buildings without the use of complex and memory demanding computational methods.

Keywords: plasters; moisture buffering; indoor moisture

1. Introduction

To regulate temperature and humidity in buildings, it is not always possible to alter the building envelope or to install air conditioning systems, especially in historic buildings, such as churches. Consequently, indoor surfaces and hygroscopic building materials are subjected to daily and seasonal temperature and Relative Humidity (RH) fluctuations, which might degrade buildings [1,2]. For these

reasons, it is important to understand the impact of temperature and humidity on buildings, as well as the response of materials to climate variations [3,4].

Indoor climate in buildings without any conditioning system is mainly determined by the outdoor climate and hygrothermal performance of the building enclosure [5]. The lack of heating and well insulated walls might generate significant daily or seasonal indoor humidity and temperature fluctuations, depending on the climate and location of the building [6,7]. The simultaneous variations of temperature and RH can produce significant variation in moisture exchange between materials and the environment [8].

Moisture transport and storage capacity of interior surface materials due to varying humidity in the indoor air is of importance both for the humidity levels of the room itself and for the moisture impact on walls surface materials [9]. There have been researches [10–13], standards [14] and some ongoing measurements on this topic [15] that pointed out the importance to understand the impact of moisture to materials durability, indoor thermal comfort and health. [16] took a step further, by considering periodic humidity variations and by applying moisture buffering experimental results into simulations. However, the focus of most of the studies was mainly on the sole RH variations, while temperature was always considered non-variable. The observation of daily indoor climate variations in non-conditioned buildings suggested a simultaneous opposite and quasi-sinusoidal temperature and RH fluctuations [6,7,17]. Some recent results on this area [1,18] gave new analytical expressions for the effect of combined variations of RH and temperature. Bylund et al. [18] analysed experimentally the moisture uptake of wood and introduced a calculation model that took into account simultaneous temperature variations together with the surface resistance of the material. However, the model was based on a specific material and required an elevated number of material properties and experimental analysis.

In a newly published study [19] a detailed analytical solution for temperature and RH square shaped variations was proposed. The method was developed by neglecting the surface vapour resistance and by considering a semi-infinite material [20]. The objective of this study was to further develop the analytical model from [19], by introducing triangular and sinusoidal temperature and RH variations. To validate the analytical method, results were compared with laboratory experimental tests on clay and gypsum plasters. The materials mass variations to simultaneous temperature and RH variations was observed and compared with simulations. The aim of this paper is to introduce new experimental approach to evaluate the moisture buffering capacity of materials and use experimental data to realistically simulate the materials behaviour. The effect of the surface resistance was implemented in the model and the validity of the semi-infinite approach on the moisture uptake was analysed. By improving the model and approximating the indoor daily variations to sinusoidal and triangular, it was possible to develop a reliable simulation method that is able to predict the materials response in a non-conditioned environment.

2. Materials

In this study commercially available undercoat clay and gypsum plasters were analysed, due to their good moisture buffering capacity. Samples were mixed and cured, as described in [21]. Clay and gypsum were cast in 150 mm x 150 mm x 40 mm and 150 mm x 150 mm x 20 mm moulds, respectively, in order to test the sensitivity of the model to the material thickness. Specimens were air dried for 28 days, before testing. The dry density ρ_{dry}, porosity $\Phi(\%)$, the dry cup water vapour resistance factor $\mu(-)$ and moisture capacity $\xi_w(kg/kg)$ were measured, as described in [21]. Results are summarised in Table 1. Materials were stored in an environmental room at 60%RH and 22^oC.

Table 1. Materials' properties and their confidence interval

Material	$\rho_{dry}(kg/m^3)$	$\Phi(\%)$	$\mu(-)$	$\xi_w(kg/kg)$
Clay	1870 ± 19	24.80 ± 4.1	19.21 ± 5.2	0.007 ± 0.003
Gypsum	856 ± 10	61.91 ± 1.5	8.84 ± 2.1	0.032 ± 0.001

3. Methods

3.1. Experimental Design

For each specimen the change in weight of the specimens was investigated, when subjected to triangular or sinusoidal simultaneous temperature and RH variations. Specimens were tested in an environmental chamber (ACS Compact Test Chambers DY110), into which a mass balance were placed to continuously measure the change in weight, as shown in Fig. 1. More details of the set-up can be seen in [8] The tests followed the general guidelines for humidity variations and test set-up of the NORDTEST protocol [14]. The materials were exposed before each tests to 24h pre-conditioning at 23^oC and 54%RH, and to six cyclic humidity and temperature variations at an air speed of 0.1 m/s. Each cycle consisted of humidity variations from 75%RH (high RH) to 33%RH (low RH), and temperature fluctuations between $18.0°C$ and $28.0°C$, which is the acceptable operating temperatures in buildings in the ASHRAE Standard 55 [22]. Temperature was set to follow inverse variation than RH, as shown in Fig. 2 and Fig. 3. For both triangular and sinusoidal fluctuation, three different humidification and de-humidification time intervals were defined, as shown in Table 2.

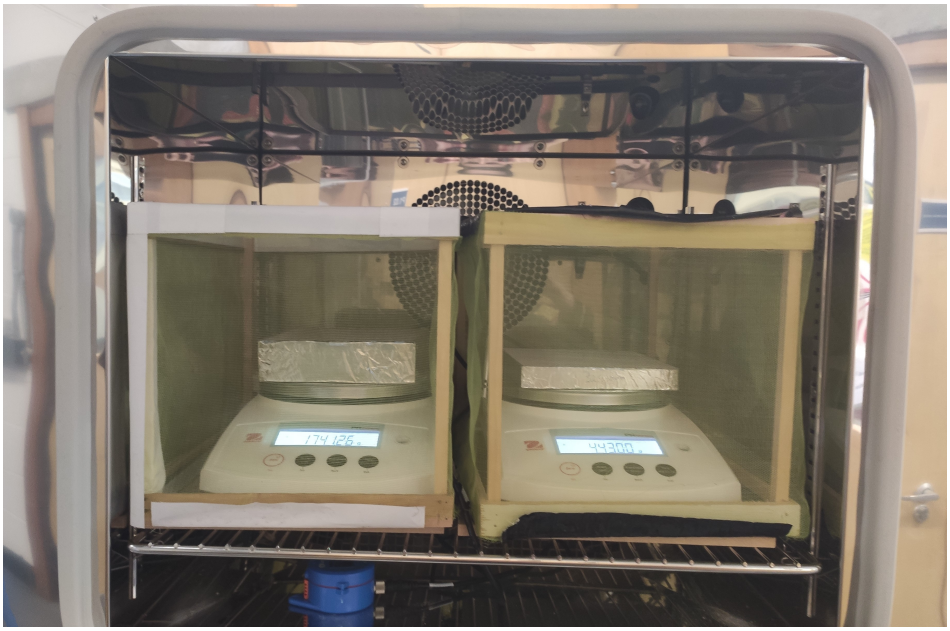

Figure 1. Moisture buffering set up in the climatic chamber

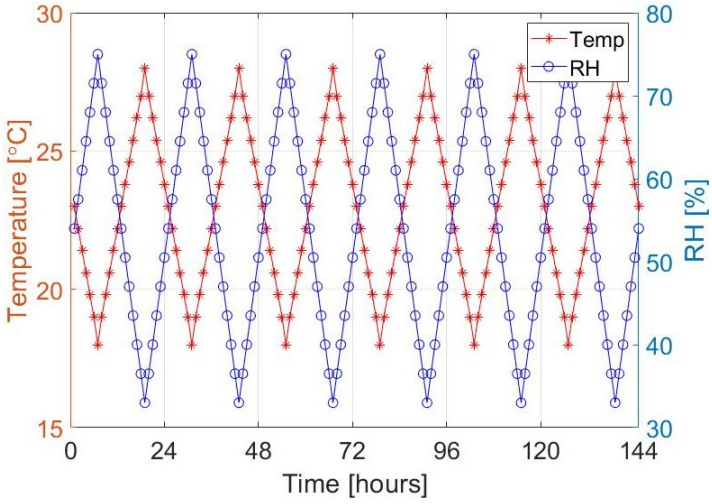

(a) Triangular 12/12h

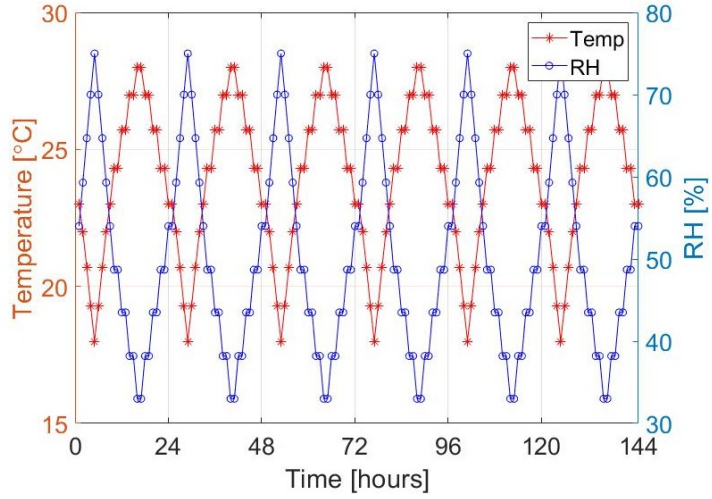

(b) Triangular 8/16h

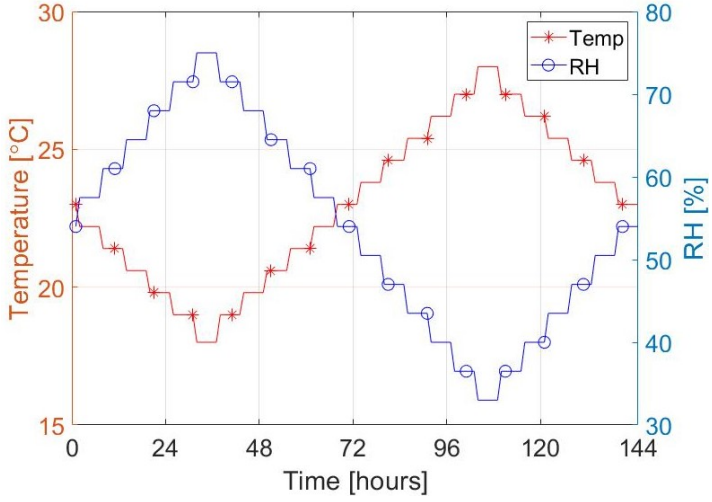

(c) Triangular 72/72

Figure 2. Triangular temperature and RH variations

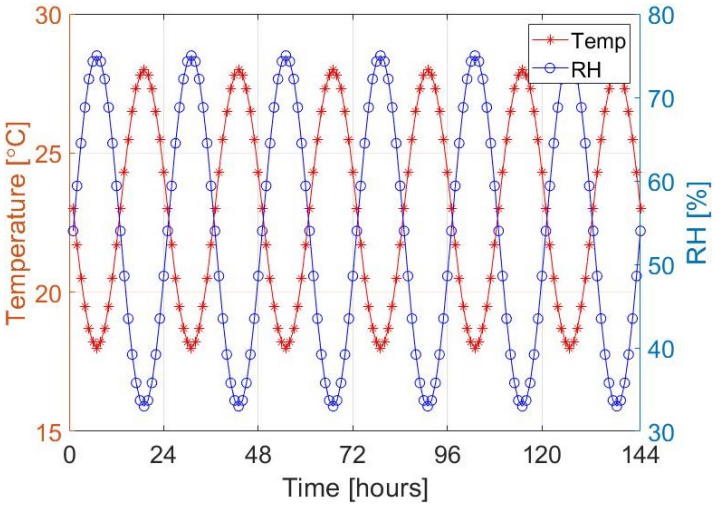

(a) Sinusoidal 12/12h

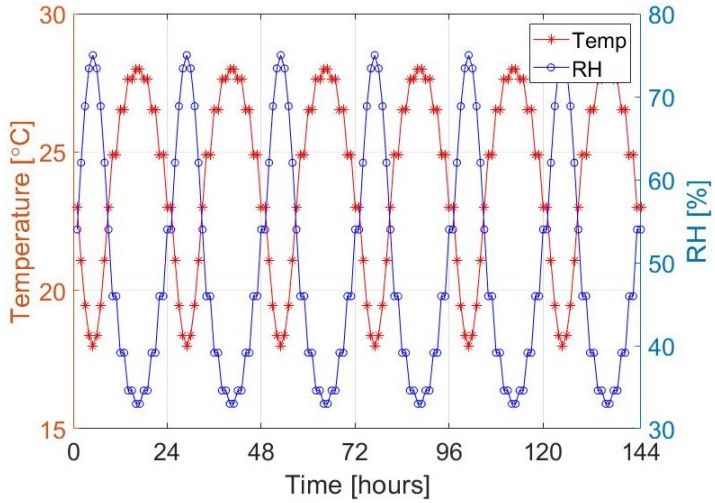

(b) Sinusoidal 8/16h

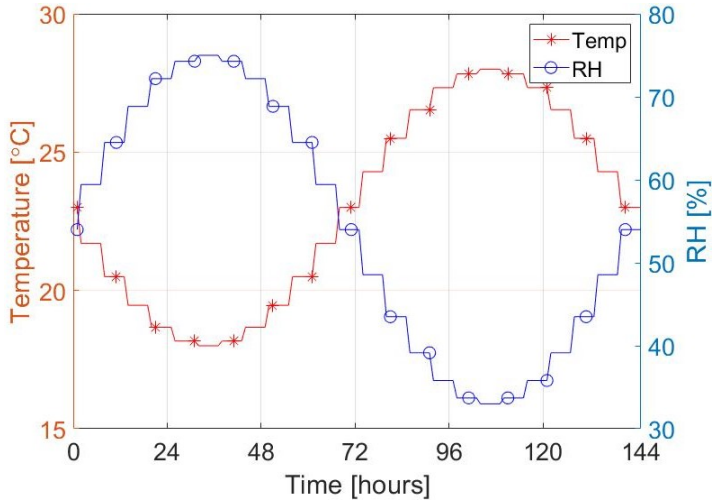

(c) Sinusoidal 72/72

Figure 3. Sinusoidal temperature and RH fluctuations

Table 2. Summary of the performed tests and time intervals for high and low temperature and RH

Tests	Temperature		RH	
	Low	High	High	Low
Triangular 12/12	12h	12h	12h	12h
Triangular 8/16	8h	16h	8h	16h
Triangular 72/72	72h	72h	72h	72h
Sinusoidal 12/12	12h	12h	12h	12h
Sinusoidal 8/16	8h	16h	8h	16h
Sinusoidal 72/72	72h	72h	72h	72h

In the *Triangular 12/12* and *Sinusoidal 12/12 tests*, considering 54%RH as starting point, the positive section of the curve represents the humidification phase, while the section below 54% is the de-humidification interval. Similarly to the NORDTEST [14], the RH was gradually increased, until reaching its maximum 75%RH and then back to 54%RH. In the first 6 hours of the de-humidification from 54%RH the humidity reached the minimum 33%RH, and then again up to 54%RH, as shown in Fig. 2a and Fig. 3a. In the *12/12* test, the climatic chamber increased and decreased the RH every hour, transitioning from one step to the other by setting a "slope", which the climatic chamber automatically generated, to progressively increase/decrease the humidity until the next RH was achieved. In the *Triangular 12/12*, the triangular curve shape was generated by creating 24 equally distributed RH intervals, while the *Sinusoidal 12/12* was achieved, by constructing a sinusoidal symmetrical equation. The temperature curve followed the same logic as the RH variations. In *12/12* test the curve started at $23°C$, reaching the minimum temperature of $18.0°C$ within the first 6 hours of the cycle. Successively, the temperature jumped back to $23°C$, to increase the temperature to $28.0°C$ always withing the 24 hour cycle. In the *Triangular 8/16* (Fig. 2b) and the *Sinusoidal 8/16* (Fig. 3b) the temperature and RH curves were marked by hourly interval in the humidification/cooling phase and by 2 hour intervals in the de-humidification/heating phase. The *Triangular 72/72* (Fig. 2c) and *Sinusoidal 72/72* (Fig. 3c) follow the same principle of the 12/12 hour fluctuations, but 6 hours intervals were applied between one step and the other, in order to understand if slower moisture variations influence the sorption capacity of the materials. A temperature and RH sensor for each specimen (Tiny Tag TV 4505) monitored the climate condition in the climatic chamber to observe the agreement between the target fluctuations and the actual measurements on both sides of the chamber. The accuracy of the sensor was $\pm 0.5^oC$ for the temperature and $\pm 3\%RH$ for humidity.

3.2. Simulations

Steady periodic variations with the time period t_p (s) in RH and temperature were investigated. The moisture transfer took place at $x = 0$ of a semi-infinite domain, $x > 0$. There was a vapour surface resistance Z (s/m) at $x = 0$. The moisture buffering effect, i.e. the total moisture m_A (kg/m^2) that flows in and then out during a time period was of interest.

3.2.1. Equations

The moisture balance equation reads:

$$-\frac{\partial}{\partial x}\left(-\delta_v \frac{\partial v}{\partial x}\right) = \frac{\partial w}{\partial t} \quad x > 0 \tag{3.1}$$

Here, v (kg/m^3) is the humidity by volume and w (kg/m^3) is the moisture content.
At the surface $x = 0$ there is:

$$-\delta_v \frac{\partial v}{\partial x} = \frac{v_b(t) - v}{Z} \quad x = 0 \tag{3.2}$$

$$-\delta_v \frac{\partial v}{\partial x} = 0 \quad x = D \tag{3.3}$$

Here, $v_b(t)$ is the time varying boundary humidity by volume. The analysis in this paper assumed that the temperature of the surface material always followed the chamber temperature $T_b(t)$ without any delay. This was a reasonable assumption since temperature changes are much more rapid than moisture changes and that it is only the thin interior surface layer that is affected by variations in indoor cyclic moisture variations. Eq. 3.3 states that there is a moisture tight back side of the material at the depth D (m) representing the thickness of the material. The main part of the following assumes a semi-infinite material thickness, i.e. $D = \infty$.

3.2.2. Simplified equations

Two simplifications were introduced. The first one is that the vapor diffusion coefficient δ_v (m^2/s) is constant:

$$\delta_v = \delta_v^0 \tag{3.4}$$

The second simplification is that the slope of the sorption curve is constant. Furthermore, hysteresis is neglected. This is justified, as the investigated materials showed a very limited difference of the slope of the isotherm within the studied RH regime. The upper and lower between the adsorption and desperation limit is 0.8% and the lower one is 0.02%. A sensitivity analysis using this span would reveal an estimate of the impact. In this paper, the average slope is used. Equation 4.8 suggest a square root dependence of the slope on the total moisture uptake.

$$\frac{\partial w}{\partial \varphi} = \xi \tag{3.5}$$

The moisture balance equation then becomes:

$$\delta_v^0 \frac{\partial^2 v}{\partial x^2} = \delta_v^0 v_s(T) \frac{\partial^2 \varphi}{\partial x^2} = \frac{\partial w}{\partial t} = \frac{\partial w}{\partial \varphi}\frac{\partial \varphi}{\partial t} = \xi \frac{\partial \varphi}{\partial t} \tag{3.6}$$

Here, v_s is the humidity by volume at saturation. Introducing the vapor moisture diffusivity a_v (m^2/s):

$$\frac{\partial^2 \varphi}{\partial x^2} = \frac{1}{a_v}\frac{\partial \varphi}{\partial t} \qquad a_v = \frac{\delta_v^0 v_s(T)}{\xi} \tag{3.7}$$

The boundary condition becomes:

$$-\frac{\partial \varphi}{\partial x} = \frac{\varphi_b(t) - \varphi}{d_v} \qquad x = 0 \tag{3.8}$$

$$d_v = \delta_v^0 \cdot Z \tag{3.9}$$

The parameter d_v(m) represents an equivalent thickness of the surface resistance, i.e. a material with this thickness gives the same resistance as Z. The boundary RH is denoted by $\varphi_b(t)$(-).

3.2.3. Varying temperature

Time varying temperature was considered:

$$\frac{\partial^2 \varphi}{\partial x^2} = \frac{1}{a_v(t)}\frac{\partial \varphi}{\partial t} \quad a_v\,(t) = \frac{\delta_v^0 v_s(T(t))}{\xi} \tag{3.10}$$

Here, the material temperature is equal to the boundary temperature. It is purely a function of time:

$$\frac{\partial^2 \varphi}{\partial x^2} = \frac{1}{a_v\,(t)} \frac{\partial \varphi}{\partial t} \tag{3.11}$$

A variable substitution is introduced:

$$\tau(t) = \int_0^t a_v(t')\, dt' \tag{3.12}$$

The moisture balance equation is transformed to:

$$\frac{\partial^2 \varphi}{\partial x^2} = \frac{\partial \varphi}{\partial \tau} \tag{3.13}$$

Here, there is an equation that is similar to the one-dimensional moisture balance equation (Eq. 3.7) with the diffusivity a_v equal to 1. The equation is linear when using this transformed time variable and superposition techniques can be used. Therefore, it is necessary with a basic periodic solution to handle complex cyclic changes in the RH.

The problem can be solved in the τ-domain using superposition technique. First, the boundary values were transformed into this domain. The following general, even functions, for the boundary RH and temperature were assumed:

$$\varphi_b(t) \quad T_b(t) \tag{3.14}$$

The maximum and minimum value of the boundary RH are:

$$\varphi_{b,\max} \quad \varphi_{b,\min} \tag{3.15}$$

The τ is defined as:

$$\tau(t) = \frac{\delta_v^0}{\xi} \int_0^t v_s(T_b(t'))\, dt' \tag{3.16}$$

Since the integrand is always positive an inverse function can be found:

$$\tau^{-1}(\tau) = t \tag{3.17}$$

The boundary RH becomes:

$$\varphi_b(t) = \varphi_b(\tau^{-1}(\tau)) = \varphi_{b,\min} + \left(\varphi_{b,\max} - \varphi_{b,\min}\right) \cdot \tilde{\varphi}_b(\tau) \tag{3.18}$$

Since a periodic and even function was assume, it becomes:

$$\tilde{\varphi}_b(\tau) = \frac{a_0}{2} + \sum_{n=1}^{\infty} a_n \cdot \cos\left(2n\pi \frac{\tau}{\tau_p}\right) \tag{3.19}$$

Where,

$$a_n = \frac{2}{\tau_p} \int_0^{\tau_p} \tilde{\varphi}_b(\tau) \cdot \cos\left(2n\pi \frac{\tau}{\tau_p}\right) d\tau \quad \tau_p = \tau(t_p) \tag{3.20}$$

This description suggested that the moisture problem, in the τ-domain, can be solved by summing an infinite number of solutions, one for each cosinusoidal variation using Fourier series. This solution is found in [10]:

$$\frac{\varphi(\tau,x)-\varphi_{b,\min}}{\varphi_{b,\max}-\varphi_{b,\min}}=\frac{a_0}{2}+\sum_{n=1}^{\infty}a_n\cdot A_n e^{-x/d_{pv,n}}\cdot\cos\left(2n\pi\frac{\tau}{\tau_p}-\frac{x}{d_{pv,n}}-\phi_n\right) \tag{3.21}$$

$$d_{pv,n}=\sqrt{\frac{\tau_p}{n\pi}}\quad \phi_n=\arctan\left(\frac{d_v}{d_{pv,n}+d_v}\right) \tag{3.22}$$

$$A_n=\frac{1}{\sqrt{(1+d_v/d_{pv,n})^2+(d_v/d_{pv,n})^2}} \tag{3.23}$$

3.2.4. Moisture uptake

The moisture flow g ($kg/m^2\cdot s$) into the material is:

$$\frac{g(t)}{\varphi_{b,\max}-\varphi_{b,\min}}=-\frac{\delta_v^0 v_s(T(t))}{\varphi_{b,\max}-\varphi_{b,\min}}\frac{\partial\varphi}{\partial x}\bigg|_{x=0}=\xi a_v(t)\sum_{n=1}^{\infty}a_n\cdot A_n\frac{\sqrt{2}}{d_{pv,n}}\cos\left(2n\pi\frac{\tau}{\tau_p}+\frac{\pi}{4}-\phi_n\right) \tag{3.24}$$

The integrated $m(t)$ (kg/m^2) moisture uptake from time zero to time t is:

$$m(t)=\int_0^t g(t')dt' \tag{3.25}$$

The formula can be reformulated using a variable substitution, $s=\tau(t)$, and an integration between 0 and τ_p.

$$m=\frac{\left(\varphi_{b,\max}-\varphi_{b,\min}\right)/2}{2\sqrt{\pi}}\xi\cdot\sqrt{\tau_p}\cdot f_m \tag{3.26}$$

$$f_m=2\cdot\sum_{n=1}^{\infty}a_n\cdot A_n\sqrt{\frac{2}{n}}\left[\sin\left(2n\pi\frac{\tau}{\tau_p}+\frac{\pi}{4}-\phi_n\right)-\sin\left(\frac{\pi}{4}-\phi_n\right)\right] \tag{3.27}$$

The moisture uptake during the uptake period becomes:

$$m_A=\frac{\left(\varphi_{b,\max}-\varphi_{b,\min}\right)/2}{2\sqrt{\pi}}\xi\cdot\sqrt{\tau_p}\cdot f_A \tag{3.28}$$

$$f_A=\max(f_{\mathrm{m}})-\min(f_{\mathrm{m}}) \tag{3.29}$$

In a dimensional analysis of the formula the different lengths that shows up can be observed. One important is the periodic penetration depth [10]:

$$d_{pv}=\sqrt{\frac{\tau_p}{\pi}} \tag{3.30}$$

The following non-dimensional parameters are of importance:

$$\frac{d_v}{d_{pv}},\frac{D}{d_{pv}} \tag{3.31}$$

On top of these two parameters, the shape of the curves for the RH and temperature boundary values, determining the Fourier Series coefficient a_n in (Eq. 3.27), is of importance.

4. Results

4.1. Experimental Results

The moisture buffering performances of clay and gypsum under triangular and sinusoidal temperature and RH fluctuations is shown in Table 3. The average peak to peak sorption capacity was calculated by considering the last three cycle of the 12h and 8h, as the changed in weight stabilised after the third cycle in all tests. In general, gypsum had a better moisture capacity than clay (Fig. 4 and Fig. 5), by adsorbing two times more moisture regardless of the shape and time interval of the temperature and RH fluctuations. The performances of gypsum were due to its porosity and pore structure. As explained in [8], gypsum presented higher porosity than clay, but it also showed a significant presence of micro-pores that increased themoisture uptake of the material. Differences between the 12h and 8h curves in the triangular case either for clay and gypsum were negligible, as the same moisture uptake was measured. Between the *Sinusoidal 12/12* and *Sinusoidal 8/16* curves 11% and 5% variations were observed for clay and gypsum, respectively. However, differences were small and not significant, when compared to the differences between triangular and sinusoidal sorption responses. There was 18% and 20% differences between *Triangular 12/12* and *Sinusoidal 12/12* peak to peak sorption capacity, while between *Triangular 8/16* and *Sinusoidal 8/16* clay and gypsum presented 10% and 13% variations, respectively. The *Triangular 72/72* and *Sinusoidal 72/72* tests presented the most significant discrepancy, as clay and gypsum adsorbed 20% and 26% more in the sinusoidal case, respectively. The considerable higher sorption capacity of the 72/72 tests is related to the longer time interval, which allowed materials to adsorb more water.

Table 3. Sorption capacity of clay and gypsum (peak to peak) for the triangular and sinusoidal temperature and RH variations

Material	Curve	Sorption $[g/m^2]$		
		12h	8h	72/72
Clay	Tri	26.69	26.33	76.34
	Sine	32.77	29.36	95.69
Gypsum	Tri	59.83	60.38	142.69
	Sine	72.25	68.47	181.07

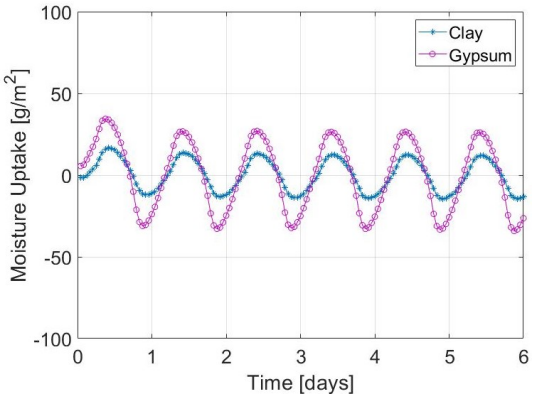

(a) Triangular 12/12h

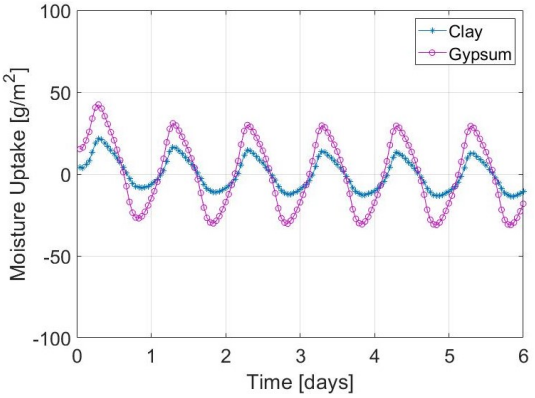

(b) Triangular 8/16h

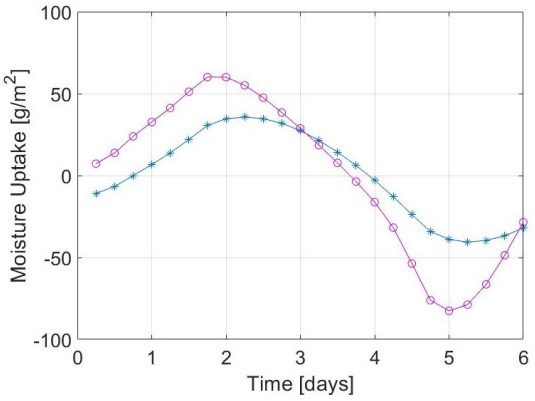

(c) Triangular 72/72

Figure 4. Moisture uptake curves for clay and gypsum under triangular temperature and RH variations

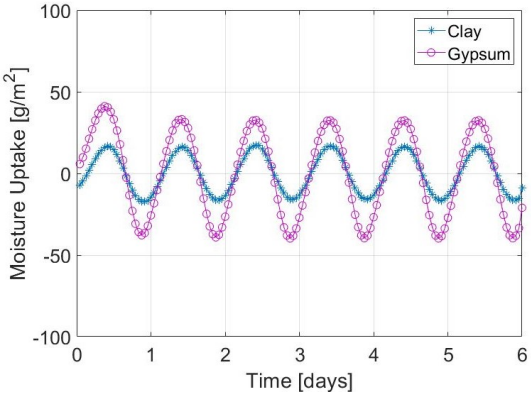

(a) Sinusoidal 12/12h

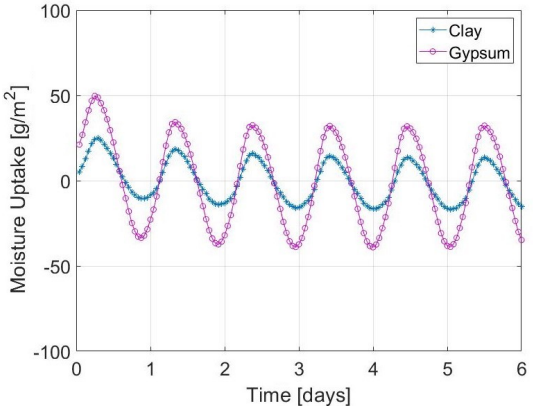

(b) Sinusoidal 8/16h

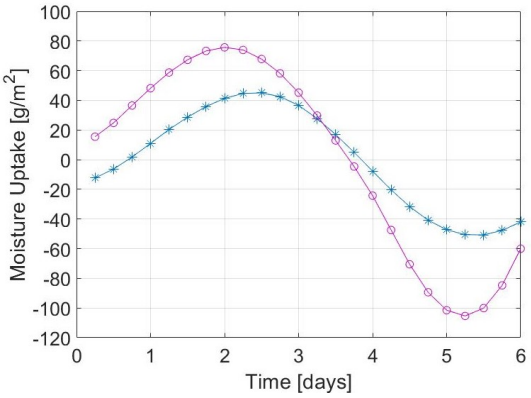

(c) Sinusoidal 72/72

Figure 5. Moisture uptake curves for clay and gypsum under sinusoidal temperature and RH fluctuations

As [8] also mentioned in a study on sinusoidal environmental variations, the triangular and sinusoidal curves presented a delayed response to the temperature and RH fluctuations (Fig. 6). The hygric lag varied depending on the humidification and de-humidification intervals, the length of each step, the material's characteristic, but especially on the simultaneous temperature variations. Table 4 summarises the hygric lags in all the tests, where the first value represents the time between the RH-peak and the moisture uptake peak, whilst the second represents the time between the lowest RH and the lowest moisture uptake value. In the Triangular and Sinusoidal 12/12 clay and gypsum showed different lags, in which clay always presented a slower response than gypsum either in the adsorption and desorption. Regardless of the materials differences, both plasters showed an asymmetry between

the humidification and de-humidification. The desorption lag was 30 minutes for clay, and 20 and 60 minutes for gypsum in the *Triangular 12/12* and *Sinusoidal 12/12*, respectively. The asymmetry indicated that in the de-humidification the response of the plasters is quicker than the adsorption, probably due to the effect of the air movement in the chamber that slowed the humidity uptake and increase the moisture release.

An opposite pattern can be seen in the *Triangular 8/16* and *Sinusoidal 8/16*, where materials presented higher hygric lags in the desorption than the adsorption. The reason could be related to the shorter humidification interval (8h) and longer de-humidification (16h), as shown in Table 4. Moreover, the the longer exposure to lower humidifies and higher temperature may slow down the moisture release. The *Triangular 8/16* the plasters had the same lag in the humidification, but in the desorption clay's delay increased significantly. In the *Sinusoidal 8/16*, clay and gypsum uptake curves had similar lags, which is in line with [8] test on the same gypsum sample.

The 72/72 test showed the biggest hygric lag, probably due to the longer steps, which allowed the materials to adsorb more moisture. In *Triangular 72/72* and *Sinusoidal 72/72* it was possible to see substantial difference between clay and gypsum. Clay was slower to adsorb water than gypsum, and it took more time to respond to the change of humidity in the air, due to its lower sorption capacity and water vapour permeability. Another important factor that might contribute to the slower response of clay was the different thicknesses of the materials. Clay was 20 mm thicker than gypsum, which means had more moisture storage capacity of gypsum with its 20 mm thickness. This is less noticeable for the 12h and 8h due to the quicker humidity variations, whilst in the 72/72 tests the specimens have got more time to adsorb water from the environment. As [23] investigated, the amount of moisture that can be adsorbed by materials is strongly dependent on their thickness and penetration depth. The penetration depth depends on the material characteristics and it determines the moisture buffering potential of materials. When the thickness of a material is smaller than its penetration depths, materials can buffer less moisture that what they potentially could adsorb.

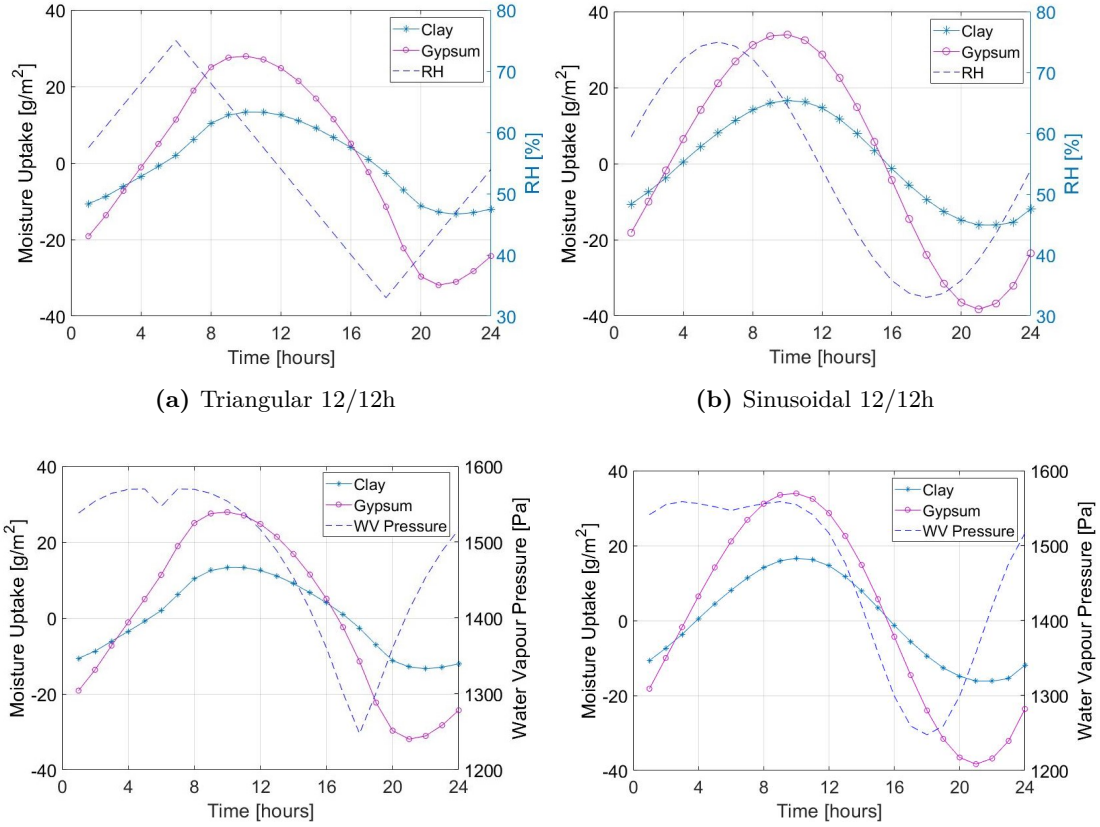

(a) Triangular 12/12h **(b)** Sinusoidal 12/12h

(c) Triangular 12/12h **(d)** Sinusoidal 12/12h

Figure 6. Hygric lag of the uptake curves for clay and gypsum under triangular (a) and sinusoidal (b) temperature and RH fluctuations, with RH as reference, and the corresponding with the vapour pressure as reference (c,d)

Table 4. Sorption hygric lag [hours]

	Triangular			Sinusoidal		
	12h	8h	72h	12h	8h	72h
Clay	4.00/3.50	2.83/4.17	18.33/21.33	3.50/3.00	2.80/4.53	21.17/21.17
Gypsum	3.00/2.67	2.83/3.33	10.67/14.17	3.33/2.67	2.80/4.80	14.17/19.83

To compare the experimental results to simulation, an uncertainty analysis was performed, to check the variability of the moisture uptake, due to experimental error. The size of the specimens and the variability of the moisture uptake were considered. The uncertainty of the single measurements were first analysed and than combined to calculate the overall variations of the moisture uptake. Table 5 shows the results of the analysis. Four measurements for each dimension were considered for the calculation of the surface area of the specimens, while three repeated moisture buffering tests were used for the climatic chamber and mass balance uncertainty calculation. Delays in the signal transmission between the mass balance and data logger were not detected.

Table 5. Uncertainty measurements

Uncertainty			Clay		Gypsum	
			Average	Uncertainty	Average	Uncertainty
Dimension	Width	mm	149.71	±0.407	150.42	± 0.016
	Length	mm	150.62	±0.795	150.41	± 0.003
	Thickness	mm	40.36	±0.008	20.94	±0.027
Area		m^2	0.023	±0.00018	0.023	±0.00018
Weight	Lows	g	576.88	±0.01	448.87	±0.03
	Peaks			±0.03		±0.07
Moisture Uptake		g/m^2	42.05	± 0.75	67.82	±1.82

The temperature and RH monitoring in the climatic chamber showed a good agreement between the actual climate conditions with the targeted curves both for the triangular and sinusoidal curves. The Triangular tests are presented in Fig. 7. In Fig. 7a the RH presented on average 2%RH variations from target, up to 5.6%RH during the de-humidification. whilst temperature showed 0.43^oC variations up to 1.40^oC. In the symmetric test (Fig. 7a) there was a better match between the actual and target climate. Temperature and RH presented an average variation of 0.17^oC and 1.50%RH, respectively, up to 0.79^oC and 3.5%RH always during the de-humidification. The temperature and RH fluctuations had smaller amplitudes than the target curves (10^oC and 42%RH), as shown in Table 6. In Fig. 7b it was also observed a delay of 1 h of RH in the de-humidification phase that was than zeroed in the humidification. The reduced RH fluctuation may produce small variations of the moisture buffering results of the two materials. Similar consideration can be done for the sinusoidal variations, as [8] explained, and as shown in Table 6.

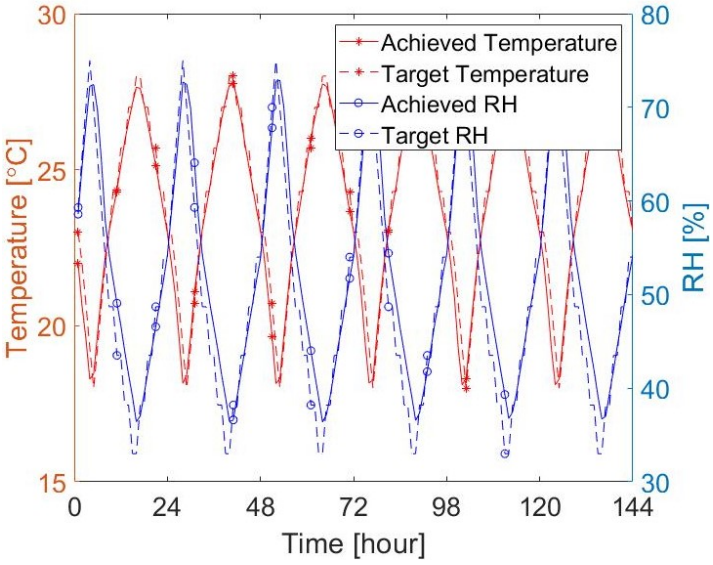

(a) Triangular 8/16h

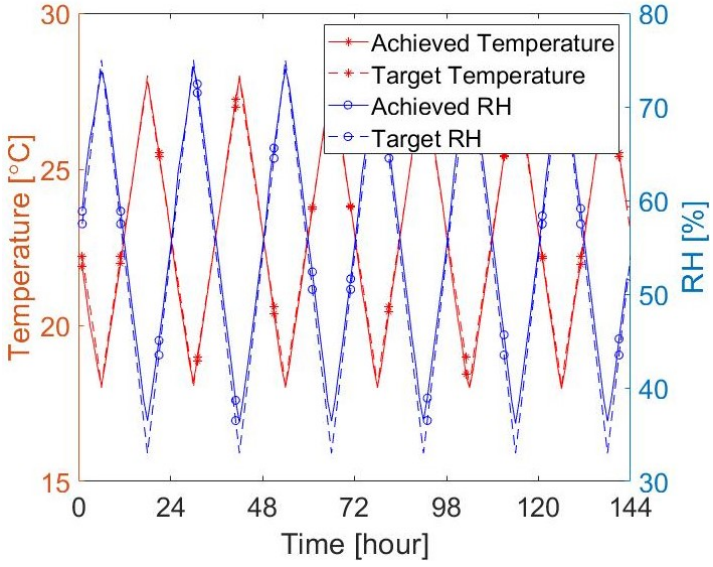

(b) Triangular 12/12h

Figure 7. Monitored temperature and RH into the chamber the triangular tests

Table 6. Temperature and RH amplitude

	Temperature	RH
Tri 8/16	9.65	36.9
Tri 12/12	9.93	38.1
Tri 72/72	9.92	39.7
Sine 8/16	9.86	37.9
Sine 12/12	9.90	39.1
Sine 72/72	9.77	39.7

4.2. Simulation results

4.2.1. Triangular 12h/12h variation for gypsum

In this section a demonstration of the application of the method is shown. As exemplification, gypsum material exposed to *Triangular 12h/12h* variation in the boundary temperature and RH-values is presented, but the analysis was performed on all cases. The following data was assumed for the vapour diffusion coefficient and the slope of the sorption isotherm:

$$\delta_v^0 = 2.828 \cdot 10^{-6} \text{ m}^2/\text{s} \qquad \xi = 27.39 \text{ kg/m}^3 \tag{4.1}$$

The time period, t_p (s) of the process is 24 h. The RH is be highest when the temperature is lowest and vice-verse. The variations are symmetrical around the average value of both the temperature and RH. The following boundary values are assumed:

$$\varphi_{b,\max} = 0.75 \quad \varphi_{b,\min} = 0.33 \tag{4.2}$$

$$T_{b,\max} = 28\,^\circ\text{C} \quad T_{b,\min} = 18\,^\circ\text{C} \tag{4.3}$$

Table 7 shows the amplitude parameterf_A (Eq. 3.28 and Eq. 3.29).

Table 7. The amplitude parameterf_A for the determination of the total moisture uptake during a half cycle, case triangular 12/12h. The third column shows the reduction in moisture buffering capacity due to the surface resistance.

Z [s/m]	f_A	$\frac{f_A}{f_A(Z=0)}$
0	2.2745	1
60	2.2203	0.98
360	1.9737	0.87
10^3	1.5708	0.69
10^4	0.3684	0.16
10^5	0.0416	0.02

From the table it is clear that for gypsum without any coating, represented by a default Z value of 360 s/m, reduces the moisture buffering capacity with 13%. In the results presented below a value of 195 s/m is used based on a assumed air velocity of 0.1 m/s and a convection surface coefficient based on forced convection [10].

The actual moisture buffering uptake is given by Eq. 3.28. For the case of zero surface resistance we have:

$$m_A = \frac{(0.75 - 0.33)/2}{2\sqrt{\pi}} 27.39 \cdot 0.0136 \cdot 2.2745 = 50.2\,\text{g/m}^2 \tag{4.4}$$

4.2.2. Simulation results for all cases, semi-infinite thickness

The periodic penetration depth (Eq. 3.30) is of interest. It must be much smaller than the thickness of the material in order to satisfy the general assumption of semi-infinite material. For gypsum and a time period of 24h:

$$\sqrt{\frac{\tau_p}{\pi}} = 0.0077 \text{ m}{=}7.7 \text{ mm} \tag{4.5}$$

For a six days time period the penetration depth is 18.8 mm. The corresponding values for clay are 7.5 and 18.5 mm for the 12h and 72h test, respectively. It means that for diurnal variations, both the thickness 20 mm and 40 mm should be applicable for the semi-infinity analysis. However, it is

questionable if the thickness of 20 mm (gypsum case) would work for the six days variation. For the thickness 40 mm (clay case) it would be acceptable.

Table 8 and Table 9 show the simulated vales for the moisture buffering uptake and the time lag. The first value for the time lag represents the time between the RH-peak and the moisture uptake peak. The second one represents the time between the lowest RH and the lowest moisture uptake value. The difference in these values clearly show the asymmetry and non-linearity of the problem. As also shown in the experimental test (Table 4), the longer lag during the de-humidification in the $8/16h$ tests, compared to the humidification can be also explained by analysing Eq. 4.8. However, the time lags in Table 9 also justify the models assumption that the surface temperature follows the room temperature. The time delay for the change in temperature in the boards, due to a room temperature change, is around 1200 s for the 20 mm thick gypsum board and 1600s for the 40 mm thick clay board. This is roughly 1/3 of an hour. For diurnal variations the ratio between this time delay and the time period is of the order 10^{-2}. For the six days period the ratio is almost one order less and can further justify the approximation.

Table 8. Simulated results for sorption capacity of clay and gypsum (peak to peak) for the triangular and sinusoidal temperature and RH variations

Material	Curve	Sorption $[g/m^2]$		
		12h	8h	72h
Clay	Tri	22.72	21.77	56.88
	Sine	27.97	26.40	69.90
Gypsum	Tri	46.50	44.45	119.25
	Sine	57.40	54.05	146.73

Table 9. Simulation results for sorption hygric lag [hours]

Hygric	Triangular			Sinusoidal		
Lag	12h	8h	72h	12h	8h	72h
Clay	2.7/2.2	2.0/2.4	15.4/12.6	3.4/2.9	2.4/3.4	19.8/16.9
Gypsum	2.9/2.3	2.2/2.6	15.9/12.9	3.5/3.0	2.5/3.5	20.0/17.2

Fig. 8 and Fig. 9 show the moisture uptake function m as a function of t/t_p. Time zero corresponds to the time of the RH peak, and the start time of integration, i.e. we assume the uptake of moisture being zero at time zero, which is an arbitrary choice of level. Consequently, it is possible to follow the accumulation and the drying out of moisture of the specimens during the time period. The two curves with the largest amplitude represent the case with a six days variation. It is clear that the diurnal variations do not significantly differ between 12/12h and 8/16h cases. As also shown in the experimental test (Table 4), the longer lag during the de-humidification in the $8/16h$ tests, compared to the humidification can be explained by analysing Eq. 4.8. If a 8/8 hours period was analysed, instead of the 8/16, the time t_p period would correspond to 16 hours. For the $16/16h$ test would be i.e. 32 hours. The difference in uptake m_A would then differ between the 8/8 and $16/16h$ approximately of $\sqrt{32/16} = \sqrt{2}$, which correspond to 40% difference. For the time delay, a pure sinusoidal variation suggests that the lag is directly proportional to the time period, which corresponds to a doubled time delay. The time delay ratio in the mixed case (8/16) in Fig. 9 is 1.17-1.62. Therefore, the asymmetry is reasonable as the delay ratio is in between 1 and 2, in line with the 8/8 and 16/16 ratio.

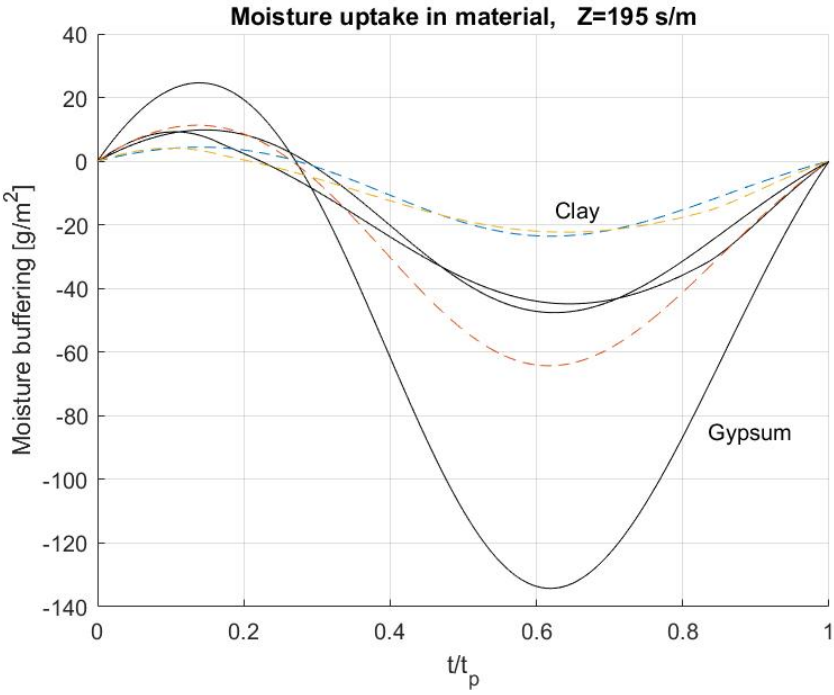

Figure 8. The moisture uptake function m (g/m^2) for the Sinusoidal variations as a function of t/t_p. The full drawn black curves represent Gypsum while the dashed ones represent Clay. The two curves with the largest amplitude represent the case with a six days variation $(72/72h)$. The smoother and more sinusoidal like curve represents $12/12h$ and the other $8/12h$, respectively.

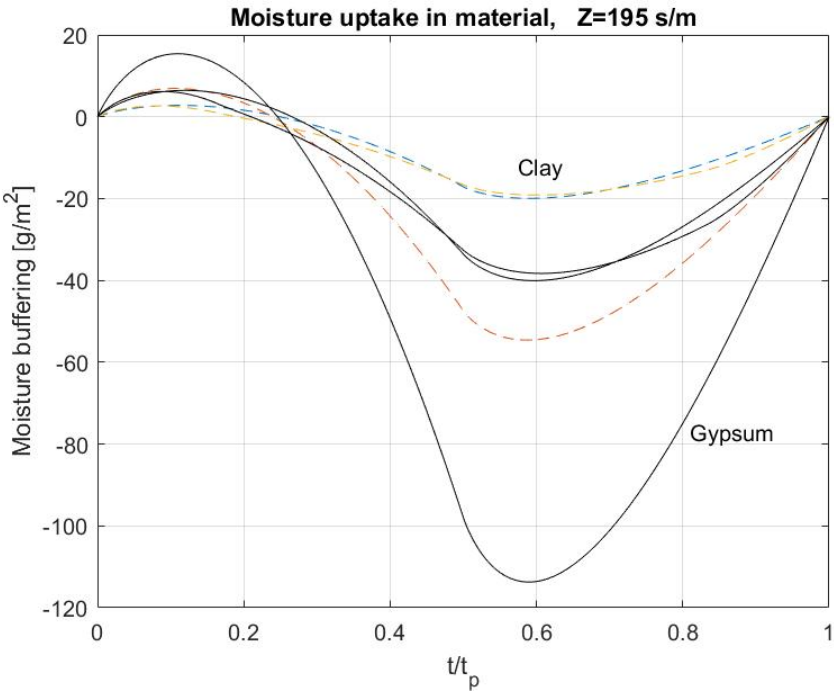

Figure 9. The moisture uptake function m (g/m^2) for the Triangular variations as a function of t/t_p. The full drawn black curves represents Gypsum while the dashed ones represent Clay. The two curves with the largest amplitude represent the case with a six days variation $(72/72h)$. The smoother and more sinusoidal like curve represents $12/12h$ and the other $8/12h$, respectively.

The comparisons with the measured data shows that the simulations systematically underestimates the moisture buffering effect by 11-37%. The largest error for the case of clay is 37% (*Sinusoidal 72/72*) and lowest 11% (*Sinusoidal 8/16*). For gypsum the differences are 36% (*Triangular 8/16*) and 12% (*Sinusoidal 8/16*). Fig. 10 shows a comparison between measured and simulated moisture uptake for gypsum and *Triangular 12h/12h cycles*.

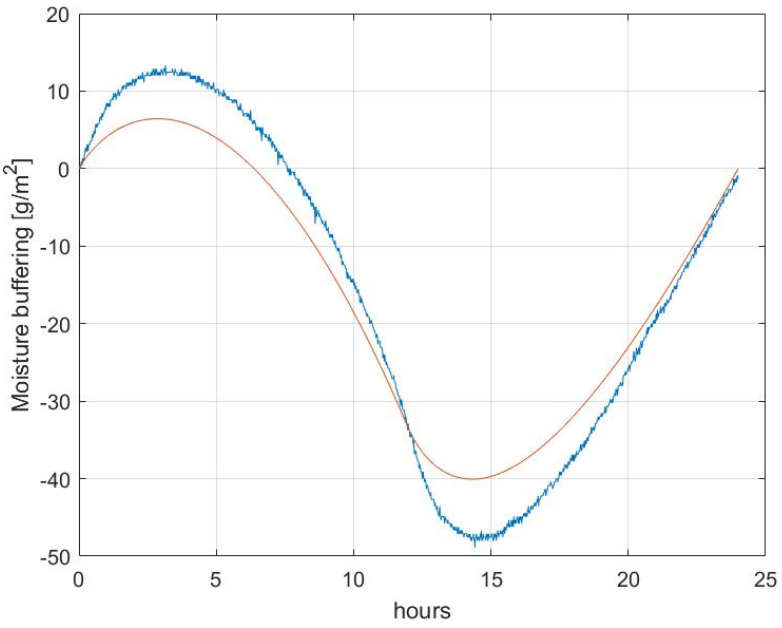

Figure 10. Comparison between measured (blue) and simulated (red) moisture uptake for Gypsum and triangular 12h/12h cycles.

4.2.3. Analysis of the simulation results

The difference between the measured and simulated results can depend on material properties, simplifications in the model, insufficient depth of samples and the assumption of the that the temperature in the material is following the boundary temperature.

Looking at the expected material dependence, from Eq. 3.28 it was obtained:

$$m_A = \frac{\left(\varphi_{b,\max} - \varphi_{b,\min}\right)/2}{2\sqrt{\pi}} \xi \cdot \sqrt{\tau_p} \cdot f_A \propto \xi \cdot \sqrt{\frac{\delta_v^0}{\xi}} \sqrt{\int_0^{t_p} v_s(T(t))\, dt} \cdot f_A \tag{4.6}$$

$$= \sqrt{\delta_v^0 \xi} \sqrt{\int_0^{t_p} v_s(T(t))\, dt} \cdot f_A \tag{4.7}$$

$$= b_v \sqrt{t_p} \sqrt{\overline{v}_s} \cdot f_A \qquad b_v = \sqrt{\delta_v^0 \xi} \tag{4.8}$$

Here, $b_v = \sqrt{\delta_v^0 \xi}$ is the moisture vapour effusivity.

The formula shows that the slope of the sorption curve and the diffusion coefficient play an equal role for the moisture uptake. The factor f_A calculated previously for all cases is not significant, as it appears to depend weakly on the RH boundary function. The same consideration applies to the square root of the integrated humidity at saturation over the time period. The previous calculation for gypsum showed that the measured value would fit if either of the parameters are increased by 66%. Considering the expression for the effusivity, it also means that a good fit happens when both material properties are increased by $\sqrt{1.66} = 1.29$ i.e. 29% increase. Fig. 11 shows the comparison between the

experimental *Triangular 12/12h* case, when this increase of the material properties is applied in the simulation.

The error estimates in relation to effusivity value gives a maximum of 13.5% higher value, not fully support a 29% higher simulation value required for a good fit. By increasing the effusivity by 66% the peak value of the experimental moisture uptake was still higher than the simulated one. The measurement uncertainty is estimated to be less than 3% which would not explain the differences between the measurement and simulations. Another potential uncertainty lies in the surface resistance value. The surface resistance value is specially important for the diurnal variations since the equivalent surface resistance thickness and the periodic penetration depth is closer in magnitude. For gypsum it is round 0.5 mm. The previous calculation shows that for a zero surface resistance, the moisture buffering effect increases by 8%.

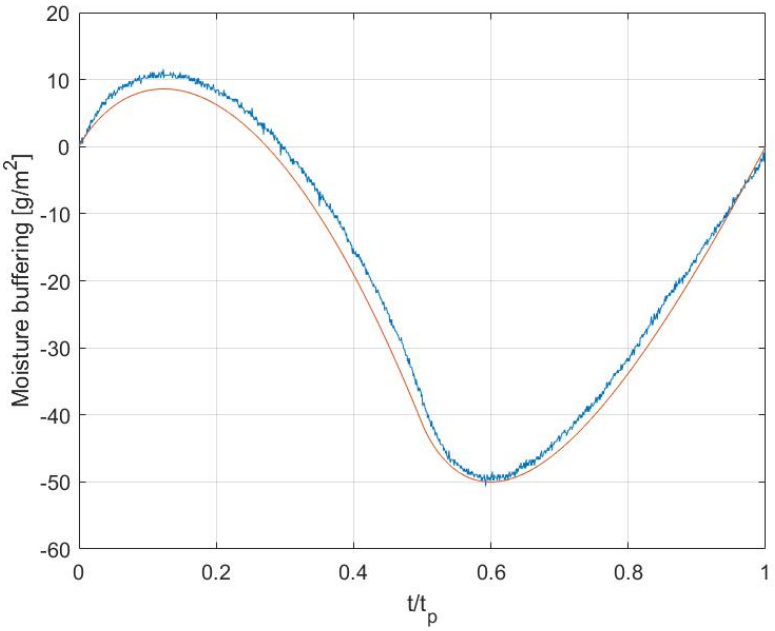

Figure 11. Comparison between measured and modified simulated moisture uptake for Gypsum and triangular 12h/12h cycles.

The only material specific part of Eq. 4.8 that gives the amplitude of the moisture uptake is the vapour effusivity b_v. By applying the same environmental variations to clay and gypsum by doubling b_v, the moisture uptake doubled. On fact, it can be observed that the ratio between the case of gypsum and clay is constant for the same load profile, following the ratio of the effusivity. The measurement give the ratio 0.45 to 0.53 while the simulations 0.48-0.49 for all cases. The variations in the simulation values are due to the small variations in f_A.

In Eq. 4.8 the term that contains the humidity at saturation depends only on the temperature variation. For a certain load profile (Tri or Sine) and time schedule (12/12h and 72/72h) this is constant. The ratio basically only depends on the square roots of the time period. Consequently, it can be expected $\sqrt{6} = 2.4494$ times greater moisture buffering effect for the 72/72h period compared to the 12/12h variation. The experimental ratio of the moisture uptake between the six days variations and 12/12h was 2.38-2.92 while simulations gave 2.50-2.56. The variations in the simulation values is due to the small variations in f_A.

4.2.4. Comparison of analytical and numerical results

In order to understand the impact of thicknesses that are close to the periodic penetration depth, numerical solutions for the equations (Eq. 3.10,Eq. 3.11 and Eq. 3.14) are presented. Only the case of gypsum was analysed. The Matlab pdepe-solver were used with a space resolution of around 0.1 mm.

From the results it can see that the semi-infinite analytical solution is verified by the numerical simulation and that it also works well for diurnal variations as long as the thickness is 20 mm or more (Table 10). For thinner material thicknesses the moisture buffering effect can be over or under estimated while the time lag becomes overestimated. It can also be observed that there is a maximum buffering effect for material thickness similar to the periodic penetration depth, which is result well known from the heat transfer area investigating effect of thermal mass on energy demand [24].

Table 10. Numerical simulation results for gypsum and varying thickness D, diurnal variations. The surface resistance $Z = 195$ s/m. Results from the analytical model is also inserted for the case of infinite thickness.

D [mm]	m_A $[g/m^2]$	$t_{delay,max}$ $[hour]$	$t_{delay,min}$ $[hour]$
5	52.0	1.67	1.08
10	64.7	3.37	2.69
20	56.7	3.57	3.05
40	57.8	3.53	3.03
100	58.1	3.48	3.05
∞	57.4	3.5	3.0

For 72/72 variations the semi-infinite analytical solution works well as long as the thickness is 40 mm or more (Table 11). For thinner material thicknesses the moisture buffering effect can be over or under estimated while the time lag becomes overestimated. The moisture buffering goes up with 14% for the 72/72 simulation with the thickness 20 mm instead of infinite thickness. This reduces the difference between experimental and simulation result.

The time lags is reduced between with 3.8 and 5.0 hours, when thickness is reduced down to 20 mm for infinity. The match between this simulation and the measurement becomes better for the top peak time delay but there is a larger lag for the bottom peak. Overall, it can be stated that either in the experimental and simulations temperature is a significant factor that delays the response of materials to buffer humidity. This is further justified in [8], in which the response of materials to constant and variable temperature were compared, showing that variable temperatures generate a significant lag compared to the case at constant temperature.

Table 11. Numerical simulation results for gypsum and varying thickness D, 72/72 variations. The surface resistance $Z = 195$ s/m. Results from the analytical model is also inserted for the case of infinite thickness.

D [mm]	m_A $[g/m^2]$	$t_{delay,max}$[hours]	$t_{delay,min}$ $[hours]$
5	57.0	1.7	1.2
10	110.5	6.3	3.9
20	167.0	16.2	12.2
40	147.7	20.6	17.7
100	146.4	20.1	17.2
∞	146.7	20.0	17.2

5. Conclusions

Clay and gypsum coatings were experimentally tested to investigate the moisture buffering capacity of the materials under simultaneous temperature and RH fluctuations. The dynamic sorption capacity of plasters were observed when environmental variations follow either sinusoidal and triangular variations

and different interval for the humidification/de-humidification were applied (12/12h, 8/16h, 72/72h). In this way, it was possible to better understand the influence of temperature and humidity on the moisture uptake of construction materials. The experimental results were compared with a novel simulation method that considers the impact of the surface resistance in the calculation of the material moisture uptake under variable environmental conditions. The model approach to consider materials as semi-infinite bodies was also verified with the analytical results.

The simulation model supported by the experimental results demonstrated clay and gypsum responded differently to the simultaneous temperature and RH fluctuations, due to the different material properties and pore structure. However, the environmental signal has a significant role in the moisture buffering capacity of materials. Both the RH and temperature signal (triangular and sinusoidal) and time intervals impact the way plasters adsorb moisture from the indoor. Differences were found when different time frames were applied. When materials were subjected to daily cycles (12/12 h and 8/16h), there were not significant differences between the sinusoidal and triangular test and also between the 12/12 h and 8/16h in terms of peak to peak sorption capacity. However, when temperature and RH were slowly varied over six days, clay and gypsum stored and released more moisture, showing also differences between the sinusoidal and triangular test. The slower increase and decrease of the environmental conditions allowed the plasters to store more moisture.

The difference between the 72h tests is linked to the different materials thickness and penetration depth. The penetration depth not only depends on the material property, but it also varies depending on the environmental conditions. For gypsum, which thickness was 20 mm, its moisture buffering performances increased in the 72h test, due to the deeper penetration of moisture into the plaster, and due to the longer exposure to high and low environmental conditions. Another observation was the lag of both plasters when exposed to simultaneous temperature and RH variations. Simulations showed a delay of few hours in the daily variations and up to 20 hours in the 72h test. The lag is attributed to temperature variations that delays the response of materials. Moreover, the continuous variations of the environmental conditions did not allow the material to stabilise and to response quickly to the humidity variations.

In conclusion, explicit analytical formulas applied in the model were derived to calculate the moisture distribution inside a material that is exposed to cyclic variations in RH and temperature. The semi-infinite analytical solution was verified, confirming the formula can be used to estimate the uptake and release of moisture to an exposed material surface as long as the periodic penetration depth is less than half the thickness of the material.

The analytical method showed a great resemblance with the measured values, and together to the novel experimental approach of testing the sorption capacity of material will quantify more accurately the capacity of hygroscopic materials to moderate the indoor humidity and improve the hygrothermal comfort and health of people in buildings.

1. Bylund Melin, C.; Hagentoft, C.E.; Holl, K.; Nik, V.M.; Kilian, R. Simulations of moisture gradients in wood subjected to changes in relative humidity and temperature due to climate change. *Geosciences* **2018**, *8*, 378.
2. Cavalagli, N.; Kita, A.; Castaldo, V.; Pisello, A.; Ubertini, F. Hierarchical environmental risk mapping of material degradation in historic masonry buildings: An integrated approach considering climate change and structural damage. *Construction and Building Materials* **2019**, *215*, 998–1014. doi:10.1016/j.conbuildmat.2019.04.204.
3. Huijbregts, Z.; Kramer, R.; Martens, M.; Van Schijndel, A.; Schellen, H. A proposed method to assess the damage risk of future climate change to museum objects in historic buildings. *Building and Environment* **2012**, *55*, 43–56. doi:10.1016/j.buildenv.2012.01.008.

4. Huijbregts, Z.; Schellen, H.; van Schijndel, J.; Ankersmit, B. Modelling of heat and moisture induced strain to assess the impact of present and historical indoor climate conditions on mechanical degradation of a wooden cabinet. *Journal of Cultural Heritage* **2015**, *16*, 419–427. doi:10.1016/j.culher.2014.11.001.
5. Napp, M.; Kalamees, T. Energy use and indoor climate of conservation heating, dehumidification and adaptive ventilation for the climate control of a mediaeval church in a cold climate. *Energy and Buildings* **2015**, *108*, 61–71. doi:https://doi.org/10.1016/j.enbuild.2015.08.013.
6. Samek, L.; De Maeyer-Worobiec, A.; Spolnik, Z.; Bencs, L.; Kontozova, V.; Bratasz, Ł.; Kozłowski, R.; Van Grieken, R. The impact of electric overhead radiant heating on the indoor environment of historic churches. *Journal of cultural heritage* **2007**, *8*, 361–369. doi:10.1016/j.culher.2007.03.006.
7. Bratasz, Ł.; Kozłowski, R.; Camuffo, D.; Pagan, E. Impact of indoor heating on painted wood-Monitoring the altarpiece in the Church of Santa Maria Maddalena in Rocca Pietore, Italy. *Studies in Conservation* **2007**, *52*, 199–210. doi:10.1179/sic.2007.52.3.199.
8. Cascione, V.; Maskell, D.; Shea, A.; Walker, P. The moisture buffering performance of plasters when exposed to simultaneous sinusoidal temperature and RH variations. *Journal of Building Engineering* **2020**.
9. Cascione, V.; Maskell, D.; Shea, A.; Walker, P. A review of moisture buffering capacity: From laboratory testing to full-scale measurement. *Construction and Building Materials* **2019**, *200*, 333–343. doi:10.1016/j.conbuildmat.2018.12.094.
10. Hagentoft, C.E. *Introduction to building physics*; External organization, 2001.
11. Svennberg, K. *Moisture buffering in the indoor environment*; Vol. 1016, Lund University, 2006.
12. Peuhkuri, R.; Rode, C. Moisture buffer value: Analytical determination and use of dynamic measurements. *IEA, ECBCS Annex* **2005**, *41*.
13. Kaczorek, D. Moisture buffering of multilayer internal wall assemblies at the micro scale: Experimental study and numerical modelling. *Applied Sciences* **2019**, *9*, 3438. doi:10.3390/app9163438.
14. Rode, C.; Peuhkuri, R.H.; Hansen, K.K.; Time, B.; Svennberg, K.; Arfvidsson, J.; Ojanen, T. Nordtest project on moisture buffer value of materials. AIVC Conference 'Energy performance regulation': Ventilation in relation to the energy performance of buildings. INIVE eeig, 2005, pp. 47–52.
15. Cascione, V.; Cavone, E.; Maskell, D.; Shea, A.; Walker, P. The effect of air velocity on moisture buffering. MATEC Web of Conferences. EDP Sciences, 2019, Vol. 282, p. 02007.
16. Zu, K.; Qin, M.; Rode, C.; Libralato, M. Development of a moisture buffer value model (MBM) for indoor moisture prediction. *Applied Thermal Engineering* **2020**, *171*, 115096. doi:10.1016/j.applthermaleng.2020.115096.
17. Xie, H.; Gong, G.; Wu, Y.; Liu, Y.; Wang, Y. Research on the hygroscopicity of a composite hygroscopic material and its influence on indoor thermal and humidity environment. *Applied Sciences* **2018**, *8*, 430. doi:10.3390/app8030430.
18. Bylund Melin, C. Wooden objects in historic buildings: Effects of dynamic relative humidity and temperature. PhD thesis, Göteborgs universitet, 2018.
19. Hagentoft, C.E. Water vapour transport to a semi-infinite material with simultaneous varying surface relative humidity and temperature. Nordic Building Physics Symposium, Tallin, 2020.
20. Hagentoft, C.E. Water vapor transport to material surfaces-Simplified analytical expressions for non-linear material properties. MATEC Web of Conferences. EDP Sciences, 2019, Vol. 282, p. 02002.
21. Cascione, V.; Maskell, D.; Shea, A.; Walker, P.; Mani, M. Comparison of moisture buffering properties of plasters in full scale simulations and laboratory testing. *Building and Construction Materials* **2020**, *252*. doi:10.1016/j.conbuildmat.2020.119033.
22. Standard, A. Standard 55–2017 Thermal Environmental Conditions for Human Occupancy. *Ashrae: Atlanta, GA, USA (2017)* **2017**.
23. Maskell, D.; Thomson, A.; Walker, P.; Lemke, M. Determination of optimal plaster thickness for moisture buffering of indoor air. *Building and Environment* **2018**, *130*, 143–150. doi:10.1016/j.buildenv.2017.11.045.
24. Ståhl, F. *Influence of thermal mass on the heating and cooling demands of a building unit*; Chalmers University of Technology, 2009.

Author Contributions: conceptualisation, V.C.,C.E.H; methodology, V.C.,C.E.H; formal analysis, V.C.,C.E.H; investigation, V.C.,C.E.H; resources, V.C.,C.E.H; data curation, V.C.,C.E.H; writing–original draft preparation, V.C.,C.E.H; writing–review and editing, V.C., D.M.,A.S.,P.W.; visualisation, V.C.,C.E.H; supervision,C.E.H D.M.,A.S.,P.W.

Acknowledgments: This study was supported by the EPSRC Centre for Decarbonisation of the Built Environment (dCarb) [grant number EP/L016869/1] and a University of Bath Research Scholarship

Conflicts of Interest: The authors declare no conflict of interest.